

# Effect of Blocking $I_{Kur}$ on the Genesis of Action Potential Alternans in Canine Atrium

Na Zhao<sup>1</sup>, Qince Li<sup>1,3</sup>, Kuanquan Wang<sup>1</sup>, Runnan He<sup>1</sup>, Yongfeng Yuan<sup>1</sup>, Henggui Zhang<sup>1,2,3,4\*</sup>

<sup>1</sup>Harbin Institute of Technology, Harbin, China

<sup>2</sup>The University of Manchester, Manchester, UK

<sup>3</sup>Peng Cheng Laboratory, Shenzhen, China

<sup>4</sup>Pilot National Laboratory of Marine Science and Technology, Qingdao, China

## Abstract

*The Kv1.5 channel-mediated, ultra-rapid delayed rectifier  $K^+$  current ( $I_{Kur}$ ) is a promising target for anti-arrhythmic drugs due to its 'atrial-selective' property. However, it is unclear yet if blocking  $I_{Kur}$  can increase the alternans susceptibility in normal atria.*

*This study aimed to investigate the effect of blocking  $I_{Kur}$  on the genesis of AP alternans associated with arrhythmogenesis. The updated canine atrial cell model developed by Ramirez *et al.* was used to implement the dynamic pacing protocol and the standard S1-S2 protocol to obtain rate dependent curves and restitution curves of AP duration (APD) and  $Ca^{2+}$  transient which were further analyzed for the alternans susceptibility.*

*Simulation results showed the prolonged AP and increased  $Ca^{2+}$  transient (CaT) by blocking  $I_{Kur}$ .  $I_{Kur}$  block from 40% to 80% produced long-short-long-short APD and  $Ca^{2+}$  transient alternans at pacing rate of ~ 2.3 Hz to 5 Hz. Further analysis showed that a possible mechanism for generating the observed alternans was due to the elevated plateau phase of AP by blocking  $I_{Kur}$ , which modulated APD and CaT via  $I_{CaL}$ . Our findings demonstrate that blocking  $I_{Kur}$  may promote the genesis of APD and CaT alternans, implying a latent pro-arrhythmic effect in normal atria.*

## 1. Introduction

The Kv1.5 channel-mediated, ultra-rapid delayed rectifier  $K^+$  current ( $I_{Kur}$ ) contributes to the early and late repolarization of the action potential (AP), of which function is prominent in atria and negligible in ventricle [1]. Therefore, it is a promising target for class III anti-arrhythmic drugs [2,3], due to the 'atrial-selective' property of the channel. Blocking  $I_{Kur}$  is thought to be a treatment for atrial fibrillation (AF) via reducing repolarization reserve that leads to prolonged action

potential duration (APD) or effective refractory period (ERP) which reduced re-entrant tendency [4,5].

With a constant pacing cycle length (CL), APD prolongation leads to shortening of diastolic interval (DI), resulting in an increased slope of the APD restitution curve. Some studies demonstrated that the steep slope of APD restitution was related to the development of APD alternans underlying the voltage-driven mechanism [6-8], even though short-term cardiac memory and calcium cycling dynamics limited predictive APD alternans by the APD restitution slope  $>1$ [9]. However, whether blocking  $I_{Kur}$  induced APD prolongation can increase the alternans susceptibility in normal atria has not yet been investigated. Therefore, this study aimed to investigate the effect of blocking  $I_{Kur}$  on the genesis of AP alternans which was associated with arrhythmogenesis.

## 2. Methods

In this study, the updated canine atrial cell model (the RNC model) developed by Ramirez *et al.* [10] was implemented to examine the effect of blocking  $I_{Kur}$  on genesis of the AP alternans. The RNC model was modified, including reducing the conductance of  $I_{to}$ ,  $I_{Kur}$ ,  $I_{Kr}$ ,  $I_{Ks}$  and  $I_{K1}$  by 10% and increasing the  $I_{NaK}$  by 30%, to maintain the APD relatively stable during the 100 beats and the action potential duration at 90% repolarization (APD<sub>90</sub>) of the 100<sup>th</sup> AP was 184.4 ms at 1Hz, which was in good agreement with experiments [11]. Then, for simulation of  $I_{Kur}$  block, the conductance of  $I_{Kur}$ ,  $g_{Kur}$ , was multiplied by 0.9 to 0.2 responding to blocking  $I_{Kur}$  from 10% to 80%.

The APD<sub>90</sub> rate dependent curve and restitutions curve were calculated using the dynamic pacing protocol and the standard S1-S2 protocol respectively [12] to analyze the genesis of AP alternans under control and  $I_{Kur}$  block conditions. Firstly, the cell model was paced at 1000 ms for 100 beats to reach relatively steady state as initial values for next simulation under control and various  $I_{Kur}$

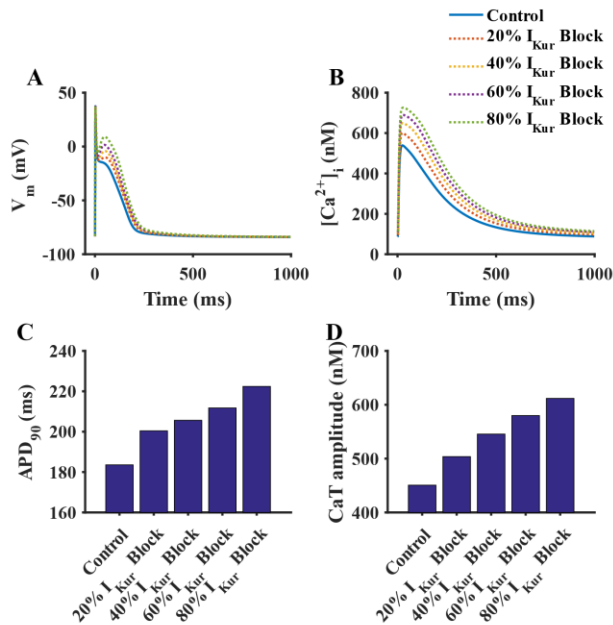


Figure 1. (A) AP morphology, (B) intracellular  $\text{Ca}^{2+}$  transient, (C)  $\text{APD}_{90}$  and (D) CaT amplitude under the control and the  $I_{\text{Kur}}$  block conditions at 1 Hz.

block conditions. Then, the two protocols were executed. In the dynamic pacing protocol, the cell model was pacing at a fixed cycle length (CL) for 100 beats to reach steady state from 1000 ms to 100 ms. The last two APs were recorded to observe whether there was an alternation with the longer and shorter AP. The APDs against different CLs constituted the APD rate dependent curve. In the standard S1-S2 protocol, the cell model was pacing at 1000 ms for 100 beats to reach steady state and then one S2 stimulus was applied after a certain diastolic interval (DI). The resulting APD of S2 stimulus was depending on DI, so that the APD against various DIs constituted the APD restitution curve.

In addition, the changes in the intracellular  $\text{Ca}^{2+}$  transient (CaT) amplitude and decay time were evaluated using the dynamic pacing protocol to obtain the CaT amplitude and CaT decay time rate dependent curves under control and  $I_{\text{Kur}}$  block conditions.

### 3. Results

#### 3.1. Effect of blocking $I_{\text{Kur}}$ on AP and CaT

Figure 1 showed the effect of blocking  $I_{\text{Kur}}$  on the AP morphology, intracellular  $\text{Ca}^{2+}$  transient,  $\text{APD}_{90}$  and CaT amplitude. The canine atrial  $\text{APD}_{90}$  at a pacing rate of 1 Hz was prolonged from 184.4 ms in the control condition to 200.4 ms, 205.6 ms, 211.7 ms and 222.4 ms in the 20%, 40%, 60% and 80%  $I_{\text{Kur}}$  block conditions, and the plateau phase of AP was elevated due to blocking  $I_{\text{Kur}}$ .

Table 1. The longest CL for the genesis of alternans in  $\text{APD}_{90}$ , CaT amplitude ( $\text{CaT}_{\text{amp}}$ ) and CaT decay time ( $\text{CaT}_{\text{DT}}$ ).

Blocking $I_{\text{Kur}}$	CL ( $\text{APD}_{90}$ )	CL ( $\text{CaT}_{\text{amp}}$ )	CL ( $\text{CaT}_{\text{DT}}$ )
0%	-	-	-
10%	-	-	-
20%	-	-	-
30%	-	-	-
40%	440 ms	-	440 ms
50%	430 ms	425 ms	435 ms
60%	400 ms	395 ms	405 ms
70%	365 ms	370 ms	375 ms
80%	330 ms	340 ms	340 ms

The CaT amplitude was increased from 450.6 nM in the control condition to 503.7 nM, 545.5 nM, 579.9 nM and 644.8 nM in the 20%, 40%, 60% and 80%  $I_{\text{Kur}}$  block conditions.

#### 3.2. APD and CaT alternans under $I_{\text{Kur}}$ block conditions

Using the dynamic pacing protocol, the  $\text{APD}_{90}$ , CaT amplitude and CaT decay time rate dependent curves were presented in Figure 2 under control and  $I_{\text{Kur}}$  block conditions (only shown 20%, 40% and 60%  $I_{\text{Kur}}$  block). Genesis of alternans was considered when the beat-to-beat variation  $> 10$  ms in  $\text{APD}_{90}$ ,  $> 10$  nM in CaT amplitude or  $> 10$  ms in CaT decay time. In the control condition (no blocking  $I_{\text{Kur}}$ ), no alternans was observed. In the  $I_{\text{Kur}}$  block conditions, no alternans was observed when  $I_{\text{Kur}}$  was blocked by from 10% to 30%, but both  $\text{APD}_{90}$  and CaT decay time alternans were observed when  $I_{\text{Kur}}$  was blocked by from 40% to 80%, and CaT amplitude alternans was observed when  $I_{\text{Kur}}$  was blocked by from 50% to 80% (beat-to-beat variation  $< 10$  nM when  $I_{\text{Kur}}$  was blocked by 40%).

Using the standard S1-S2 protocol, the  $\text{APD}_{90}$  restitution curve were presented in Figure 3 under control and  $I_{\text{Kur}}$  block conditions (only shown 20%, 40% and 60%  $I_{\text{Kur}}$  block). The maximum slope in the control and the 20%  $I_{\text{Kur}}$  block conditions were 0.48 and 0.8 which were  $< 1$  corresponding to no alternans of rate dependent curves in Figure 2 and Table 1. The maximum slope in the 40% and 60%  $I_{\text{Kur}}$  block conditions were 1.46 and 2.54 which were  $> 1$  corresponding to alternans of rate dependent curves in Figure 2 and Table 1. When  $I_{\text{Kur}}$  was blocked by 40%, the DI with maximum slope was 320 ms and the resulting  $\text{APD}_{90}$  of the S2 stimulus was 154 ms so that the CL was 474 ms. When  $I_{\text{Kur}}$  was blocked

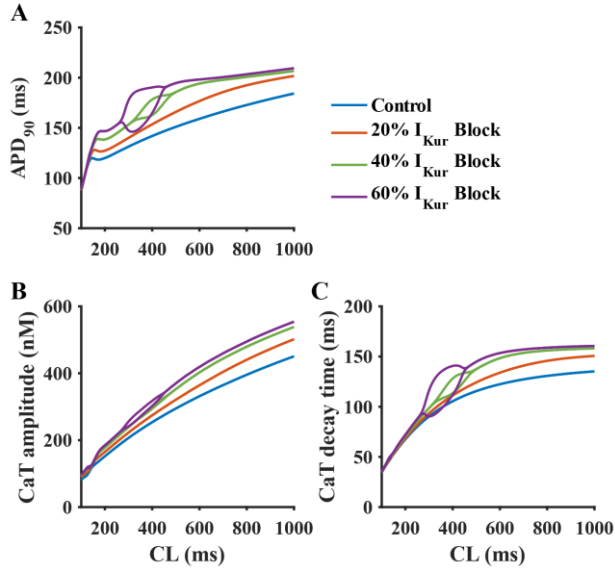


Figure 2. (A) APD<sub>90</sub>, (B) CaT amplitude and (C) CaT decay time rate dependent curves obtained using the dynamic pacing protocol under control and  $I_{Kur}$  block conditions.

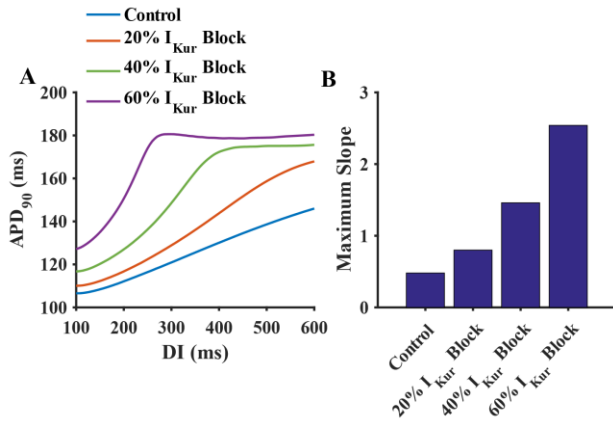


Figure 3. (A) APD<sub>90</sub> restitutions curves obtained using the standard S1-S2 protocol under control and  $I_{Kur}$  block conditions. (B) The maximum slopes of the APD<sub>90</sub> restitution curves in (A).

by 60%, the DI with maximum slope was 234 ms and the resulting APD<sub>90</sub> of the S2 stimulus was 167ms so that the CL was 401 ms, which was shorter than the one in 40%  $I_{Kur}$  block condition.

### 3.3. Mechanism of alternans under $I_{Kur}$ block conditions

Further analysis for the mechanism of alternans under  $I_{Kur}$  block condition was demonstrated in Figure 4 which showed the alternans of AP, intracellular CaT,  $I_{Kur}$ , L-type calcium current ( $I_{CaL}$ ) and its voltage-dependent activation

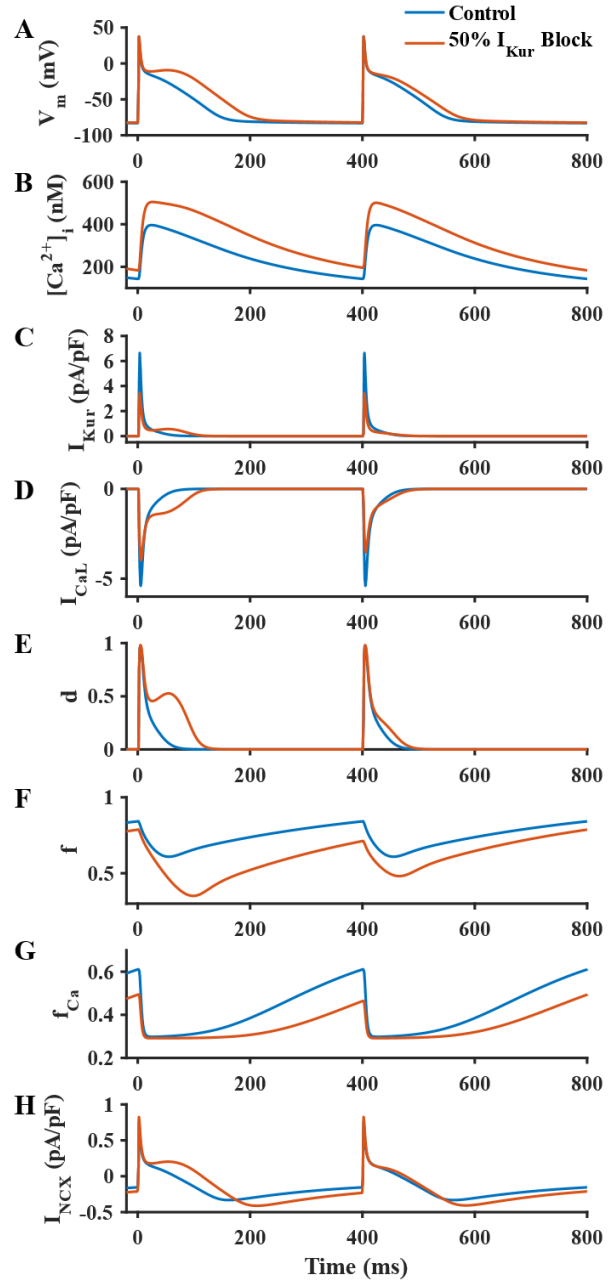


Figure 4. Alternans of (A) AP, (B) intracellular CaT, (C)  $I_{Kur}$ , (D)  $I_{CaL}$ , (E)  $d$ , (F)  $f$ , (G)  $f_{Ca}$ , and (H)  $I_{NCX}$  at a pacing CL of 400 ms in control and 50%  $I_{Kur}$  block condition.

gate ( $d$ ), voltage-dependent inactivation gate ( $f$ ) and calcium-dependent inactivation gate ( $f_{Ca}$ ), and Na-Ca exchange current ( $I_{NCX}$ ) at a pacing CL of 400 ms in control and 50%  $I_{Kur}$  block conditions. The alternans was in-phase. The longer APD was accompanied by a larger CaT amplitude and slower rate of decay. The shorter APD was accompanied by smaller CaT amplitude and faster rate of decay (Figure 4A and 4B).

In the long AP, the plateau phase of AP was elevated

and prolonged by blocking  $I_{Kur}$ , which led to extended open time of the  $I_{CaL}$  voltage-dependent activation gate (Figure 4E) resulting in increased transmembrane  $Ca^{2+}$  influx through  $I_{CaL}$  (Figure 4D). More  $Ca^{2+}$  influx increased the CaT amplitude and slowed the decay time of  $Ca^{2+}$  transient, so that before the next AP intracellular  $Ca^{2+}$  did not completely recover to diastolic level. Therefore, the value of calcium-dependent inactivation gate of  $I_{CaL}$  was smaller (Figure 4G) before the next AP resulting smaller  $I_{CaL}$  of the next AP (Figure 4D). In addition, due to the long AP, voltage-dependent inactivation gate of  $I_{CaL}$  did not completely recover to the level before this AP (Figure 4F) resulting smaller  $I_{CaL}$  of the next AP. The consequent smaller  $I_{CaL}$  shortened the AP and the plateau phase resulting reduced open time of the  $I_{CaL}$  voltage-dependent activation gate and decreased transmembrane  $Ca^{2+}$  influx that led to the short AP, small CaT amplitude and fast rate of CaT decay. Moreover, the alternans of  $Ca^{2+}$  transient caused alternans of  $I_{NCX}$  which played a significant role in AP repolarization (Figure 4H).

#### 4. Discussion and conclusion

In this study, the updated canine atrial cell model was used to investigate the effect of blocking  $I_{Kur}$  on the genesis of AP alternans. In this simulation, blocking  $I_{Kur}$  from 40% to 80% produced noticeable long-short-long-short APD and CaT alternans at pacing CL of ~ 200ms to 440 ms. At these pacing CL, the slope of DI-dependent APD<sub>90</sub> restitution curve was steeper which was responsible for the genesis of AP alternans. Further analysis for the mechanism of alternans was demonstrated that the elevated plateau phase of AP by blocking  $I_{Kur}$  played a significant role in  $I_{CaL}$  which modulated APD and CaT. Such simulation results are in consistence with experimental data obtained from rabbit atrial cells showing that alternation in AP morphology contributed to atrial alternans via  $I_{CaL}$  [13].

In conclusion, this study demonstrates that although prolonging the APD, blocking  $I_{Kur}$  may promote the genesis of AP alternans, implying the latent pro-arrhythmic effect in normal atria.

#### Acknowledgments

The work is supported by the National Science Foundation of China (NSFC) under Grant Nos. 61572152 (to HZ), 61571165 (to KW), 61601143 (to QL) and 81770328 (to QL), and China Postdoctoral Science Foundation under Grant Nos. 2015M581448 (to QL).

#### References

[1] U. Ravens and E. Wettwer, "Ultra-rapid delayed rectifier

channels: molecular basis and therapeutic implications," *Cardiovascular research*, vol. 89, no. 4, pp. 776-785, Mar. 2011.

- [2] J. Ford, et al., "The positive frequency-dependent electrophysiological effects of the  $I_{Kur}$  inhibitor XEN-D0103 are desirable for the treatment of atrial fibrillation," *Heart Rhythm*, vol. 13, no. 2, pp. 555-564, Feb. 2016.
- [3] S. Loose, et al., "Effects of  $I_{Kur}$  blocker MK-0448 on human right atrial action potentials from patients in sinus rhythm and in permanent atrial fibrillation," *Front. Pharmacol*, vol. 5, Article.26, Mar. 2014.
- [4] N. Schmitt, M. Grunnet, and S.P. Olesen, "Cardiac potassium channel subtypes: new roles in repolarization and arrhythmia," *Physiol Rev.*, vol. 94, no. 2, pp. 609-653, 2014.
- [5] M. Lei, L. Wu, D.A. Terrar, and C.L.H. Huang, "Modernized classification of cardiac antiarrhythmic drugs," *Circulation*, vol. 138, no.17, pp. 1879-1896, 2018.
- [6] Z. Qu, A. Garfinkel, P.S. Chen, and J/ N. Weiss, "Mechanisms of discordant alternans and induction of reentry in simulated cardiac tissue," *Circulation*, vol. 102, no. 14, pp. 1664-1670, 2000.
- [7] J. I. Goldhaber, et al., "Action potential duration restitution and alternans in rabbit ventricular myocytes: the key role of intracellular calcium cycling," *Circ Res.*, vol. 96, no. 4, pp. 459-466, 2005.
- [8] M.L. Koller, et al., "Altered dynamics of action potential restitution and alternans in humans with structural heart disease," *Circulation*, vol. 112, no. 11, pp. 1542-1548, 2005.
- [9] J.M. Weiss, et al., "From pulsus to pulseless: the saga of cardiac alternans," *Circ Res.*, vol. 98, no. 10, pp. 1244-1253, 2006.
- [10] R.J. Ramirez, S. Nattel, and M. Courtemanche, "Mathematical analysis of canine atrial action potentials: rate, regional factors, and electrical remodeling," *Am J Physiol Heart Circ Physiol*, vol. 279, no. 4, pp. H1767-H1785, 2000.
- [11] Y.H. Yeh, et al., "Calcium-handling abnormalities underlying atrial arrhythmogenesis and contractile dysfunction in dogs with congestive heart failure," *Circ Arrhythmia Electrophysiol.*, vol. 1, no. 2, pp. 93-102, 2008.
- [12] W. Wang, et al., "Mechanistic insight into spontaneous transition from cellular alternans to arrhythmia-A simulation study," *PLoS Comput Biol*, vol. 14, no. 11: e1006594, 2018.
- [13] G. Kanaporis, L. A. Blatter, "Membrane potential determines calcium alternans through modulation of SR  $Ca^{2+}$  load and L-type  $Ca^{2+}$  current," *Journal of Molecular and Cellular Cardiology*, vol. 105, pp. 49-58, 2017.

Address for correspondence:

Henggui Zhang.  
92 West Dazhi Street, Nangang District, Harbin, China  
henggui.zhang@manchester.ac.uk